A Compact Soft Articulated Parallel Wrist for Grasping in Narrow Spaces

F. Negrello[1], S. Mghames[2], G. Grioli[1], M. Garabini [2], M. G. Catalano[1]

Abstract—

The increasing presence of high density logistic warehouses demands the deployment of fast and flexible robotic solutions. One of the open challenges towards this objective is manipulation in narrow settings. This work addresses such a problem from a design perspective. By observing human arm dexterity and grasp strategies, the role of the wrist emerges as fundamental in providing both a large workspace and a minimal clearance. We compare the kinematic envelope of robotic manipulators wrist to their human counterpart through the introduction of the *reversed workspace*, defined as the volume required by a kinematic chain for a set of end-effector orientations. Results suggest to combine the properties of serial and parallel architectures, to obtain a suitable trade-off between compactness and workspace. On this base, we present a novel soft articulated parallel wrist device that can be easily interfaced with industrial off-the-shelf manipulators to enhance their manipulation capabilities in constrained environments.

I. INTRODUCTION

Despite present research efforts of both large logistic companies (Amazon picking challenge), and academics (SOMA, ROBLOG, Second Hand)[1], the complete automation of packaging and distribution processes is still an open problem. In particular the aspect of grasping in narrow and constrained spaces, such as shelves, boxes or containers, is not solved by robotic manipulators, which are still far from matching human skills in terms of dexterity, speed and reliability. To enhance the manipulation capabilities of a robotic system in narrow spaces, one of the fundamental aspects to be understood is the correlation between degrees of freedom (DOFs) of a kinematic structure and its dexterity. Several authors, as Ma and Dollar in [1], suggest to enhance end-effector dexterity to overcome the restrictions posed by environmental constraints and arm limitations (i.e. singularities). Also recent studies on human grasp provide insights on how to improve robot capabilities, highlighting that during human manipulation and grasp, a large variety of contacts with the environment are observed [2] and suggesting grasping approaches capable of leveraging on such aspects [3][4]. This contributed to the interest towards hands with compliant

Fig. 1: Examples of robot grasping in a box with and without the Compact Soft Articulated Parallel Wrist (SWR).

and adaptive behaviors [5]. The majority of these previous works focus on the role and importance of the hand alone, despite the fact that, there are evidences on how the wrist-hand ensemble plays a fundamental role in the grasping phase [6][7]. These evidences become more and more crucial when facing tasks such as grasping in narrow spaces. Active wrists notoriously improve robot manipulation capabilities as they allow to rotate the end-effector to align with the orientation of the task. To provide full capability, at least three orientation DOFs are required to the wrist. Typical solutions to implement them in robotics include spherical serial R-P-R wrists, but more recently, also non-concurrent axes design started to become more established because of their smaller footprint. Traditionally, robotic manipulators and grippers have been designed for table-top operation, i.e. tasks where there are no significant constraints to the robot motion. In these conditions, non-spherical wrist kinematics (e.g. Panda, UR)[2], compared to a spherical ones (e.g. Kuka LWR), can offer several advantages: they have no singularity in fully stretched position, are easily implemented with a serial chain and, most important, are more compact than the equivalent serial spherical configuration. Unfortunately, real world scenarios, are much more complex than simple table-top operation: objects are often tightly packed (Fig. 2), and the most relevant problem, rather than planning for the best grasp, becomes how to reach the object [8]. One of the main challenges is given by the set of constraints (box size and object location) that limit the poses that the end-effector can reach, therefore hindering the overall system workspace and dexterity [9] [10]. This set of challenges define the *grasp in a box problem*. Intuitively, the dexterous workspace of a compact wrist would be less affected by box constraints.

[1] http://soma-project.eu, http://roblog.eu, http://secondhands.eu,

[2] www.franka.de, www.universal-robots.com, www.kuka.com

Fig. 2: Examples of shelves and container commonly used in groceries, houses, logistics warehouses and supermarkets.

To this purpose, in section II we introduce the *Reversed Workspace* as novel index to quantify the volume required by a kinematic chain for a set of end-effector orientations. This led the authors to think that the combination of compact spherical compliant kinematics and soft adaptive hand, could represent an important step forward, improving the grasping capabilities of robots in narrow spaces. In addition, this work presents a novel soft articulated[3] robotic wrist device (SWR in Fig. 1) which can be easily interfaced with industrial off-the-shelf manipulators and modern compliant hands. The starting point of this study is the definition of design criteria based on the manipulators and human wrist kinematics.

Aiming to design a compact wrist solution, we compare the *reversed workspace* of different manipulators presented in literature, with that of the average human. Results suggest that serial kinematic chains have an extended dexterous workspace while parallel mechanisms allow to shape by design the center of rotation of their links, enabling the development of compact mechanisms.

On this base, we developed a 2DOFs SEA parallel module, inspired by [12][13], which can be connected to a serial manipulator to combine the properties of serial and parallel architectures, providing a suitable trade-off between compactness and workspace. Literature on compliant parallel architectures is scarce, some examples are provided by [14][15] which adopt linear actuators, therefore their form factor is not suitable for our purposes. This work presents the design study, development, and characterization of the compact soft articulated parallel wrist, accompanied by a set of grasping tests in several box-like scenarios for demonstrating the effectiveness of the proposed design. Note that, with this approach, robot redundancy is increased by 2DOFs, a study on control strategies to advantageously manage it requires further discussion which is beyond the scope of this work.

The paper is structured as follows, in Sec. II we provide context to the *grasp in a box* problem comparing the *reversed workspace* of human and state of art manipulators wrists. In Sec. III the design concept, model and prototype of the Soft Articulated Compact Parallel Wrist is presented. Finally, Sec. IV-V report the system experimental characterization and its testing in industrial-like scenarios.

II. ARTIFICIAL AND HUMAN WRIST KINEMATICS

In the *grasp in a box* task, the box sets the operational space constraints in which the robot should move. The space required by a robot to achieve a given end-effector pose (or

[3]according to the definition of *soft articulated robots* provided in [11]

trajectory) is defined by its kinematic envelope. The task is feasible if a kinematic envelope exists, such that the end-effector pose can be reached, subject to the operational space constraints. Intuitively, the smaller is the robot envelope, the highest are the chances to find a feasible solution to accomplish the task. The kinematic envelope of a robot is defined by two factors, namely the actuation volume and its kinematics, which defines where the actuators are located and how are connected. Concerning the kinematic chain, it depends on joints types and their location. The actuation volume, instead, it is defined by the actuator and transmission design, and is optimized maximizing its power density. This is a well-known engineering problem, which we do not further discuss. The former considerations can be formalized in the following problem: to determine the kinematic chain that minimizes a manipulator's envelope for the set of poses required for the *grasp in a box* task (*reversed workspace*).

Consider a generic serial robot arm with a given end-effector. The robot arm kinematics can be parametrized by the Denavit-Hartemberg convention, and position of each link can be found by concatenating relative transformation matrices $R_i^{i-1}(a_d, q_k)$ as in

$$A_i^0 = \prod R_i^{i-1}(a_d, q_k), \qquad (1)$$

where $q_k \in \mathbb{R}$ represents the joint configuration vector for the $k - th$ pose, and a_d represents the vector of geometric parameters of the $d - th$ design. Given the task under analysis, a suitable choice is to consider a kinematic chain starting from the object to be grasped (0-th link) and then including the robot links in a reverse order, from the end-effector (1st link) to the robot base ($n + 1$-th link). Let us consider a set of L desired end-effector poses described by $\{A_{1,\ell}^0\}$ $\ell \in \{1, ..., L\}$. Said $P_i = \{p_i^0(a_d, q_k)\}$ the set of points of the $i - th$ link for a given configuration q_k, the robot envelope E is given by

$$E = \bigcup_i P_i^0, \qquad (2)$$

where each point p_i^0 depends on the robot configuration according to

$$p_i^0(a_d, q_k) = A_i^0(a_d, q_k)p_i^i. \qquad (3)$$

Assume that the operational workspace can be limited by a set of linear constraints in the operational space $C = \{c_j\}$ such that $c_j^T p_i(a_d, q_k) < 0$. Notice that this assumption holds for several practical cases, e.g. the *grasp in a box* task. Hence, the problem of choosing the $d - th$ design meta-parameters that minimize the robot reversed workspace can be formalized in the following optimization problem

$$\begin{aligned} \min_d \quad & E \\ s.t. \quad & c_j^T p_i(a_d, q_k) < 0 \quad \forall i, j \\ & p_{n+1}^0 = A_{n+1,\ell}^0 p_{n+1}^{n+1} \quad \forall \ell \end{aligned} \qquad (4)$$

Due to the nonlinear dependence of $p_i(a_d, q_k)$ on a_d and q_k the problem (4) is in general not convex and not easily approachable. To tame its complexity we considered only the
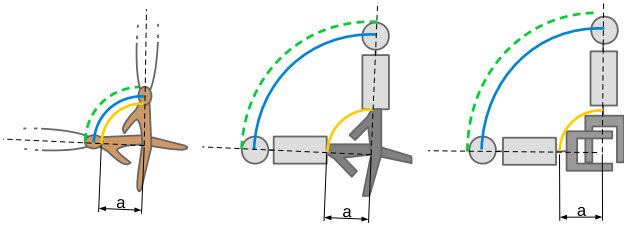
Fig. 3: Examples of 2D reversed workspace of human wrist and robotic manipulators with different end-effector morphology. Yellow curve is the hand/end-effector envelope, blue curve is the wrist reference frame envelope, the green curve represents the overall wrist envelope, which considers also the physical manipulator size.

last link of the wrist. Therefore, the wrist *reversed workspace* coincides with the workspace of the reference frames of the wrist links evaluated with respect to fixed end-effector frame. To explain our approach, Fig. 3 shows the 2D reversed workspace of a human wrist and two robot manipulators. The yellow curve describes the hand/end-effector envelope, the blue curve is the envelope described by the wrist reference frame, where finally, the green curve represents the overall wrist envelope, which considers also the physical manipulator size. Note that, for the human wrist the three envelopes are almost superimposed. From anthropometric data length [16], the averaged human hand is about 92mm (a in Fig. 3), and represents a reference for our analysis.

The analysis ranges over different kinematic schemes of industrial manipulators retrieved in literature (Fig. 4 e-h). Among other parallel structures, the hybrid serial-parallel spherical mechanism (Fig. 4g) was considered since it allows to obtain a spherical joint with a workspace close to the human wrist and allows easily to relocate the actuation mass to reduce power requirements of proximal DOFs [13]. Although the study aimed for generality, many parameters and details depend on the specific implementation, and usually multiple implementations exist to reproduce the same kinematic scheme [17]. It is possible that other mechanisms with similar performances exist, and the reversed workspace allows to evaluate their similarity, while a deep classification of wrist kinematic layouts exceeds the purpose of this work. Fig. 4 reports the wrist reversed workspace of the considered kinematic schemes, evaluated for different end-effector orientations, 0-90° azimuth and elevation angle. In Fig. 4 the end-effector frame is located at (0 0 0). Note that each configuration of a spherical R-P-R wrist is described by a single point of the reversed workspace. Therefore, the radius of the sphere represents the main characteristic dimension of the reversed workspace. Consequently, the reversed workspace of kinematics in fig. 4(a) and 4(d) is a sphere octant, like the end-effector envelope. On the other hand, for non-spherical configurations, to a single end-effector orientation are associated multiple links position (a circumference), therefore the corresponding reversed workspace is a larger portion of a sphere. Figs. 4(b) and 4(c) report the reversed workspace of two non-spherical layouts. Note that, despite the radius of both of them is smaller

than that of the spherical R-P-R configuration the overall reversed workspace is similar. The hybrid serial-parallel spherical mechanism (fig. 4(d)), proposed in [13], compared to the serial architecture discussed above, provides the most compact reversed workspace, being almost equivalent to the end-effector envelope, similarly to the human wrist. A full 3DOFs parallel mechanism, can be optimized to locate the wrist rotation center exactly at the end-effector reference frame [18]. In this particular condition, the wrist envelope would be defined only by end-effector size. Drawbacks of a pure parallel mechanism would be an increased system complexity (larger number of links) and a reduced range of motion due to links interference and platform singularities [19]. Concluding, we evaluated several kinematic chains with similar workspaces, and the hybrid serial-parallel joint resulted the best choice for compact wrist design, providing the *reversed workspace* that fits best the human reference.

III. COMPACT SOFT PARALLEL WRIST DESIGN

A. Concept

The grasp in a box problem identifies three main design requirements for designing a wrist:

High dexterity: increase the capability of re-orienting the end-effector by adopting a spherical wrist.

Compact structure: reduce the reversed workspace integrating a parallel architecture on a serial manipulator.

Adaptiveness: capability to adapt to environmental constraints by the introduction of compliant elements. A positive side effect of this approach is an increased system robustness.

Moreover, to guarantee full compatibility with existing industrial manipulators, we envision a fully integrated 2DOFs add-on module which, combined with the last DOF of the manipulator, provides the complete 3DOFs Hybrid joint kinematics.

B. Kinematics

The 2DOFs spherical mechanism adopted for the compact soft articulated wrist (Fig. 5(a)), is based on the 2DOFs agile eye [12]. Its closed form kinematics is reported below, (for a detailed analysis of the mechanism kinematics refer to [13]). It consists of 2 serial chains with a total of 3 passive joints (light grey joints in Fig. 5(a)). The first chain is represented by frames $\{Z_0, Z_1, Z_3, Z_7\}$ in Fig. 5(a) while the second is represented by $\{Z_0, Z_2, Z_4, Z_5\}$. We define $\dot{q}_p \triangleq [\dot{q}_1 \ \dot{q}_2]^T$ as the angular velocities of the active joints, and $\phi_{1,2,3}$ as the Euler angles defining rotations about $\{X_0, Y_0, Z_0\}$ which, based on the literature of artificial wrists [7], correspond to pitch, yaw and roll angles of the end-effector, respectively. Given the active joints orientations $\{q_1, q_2\}$, the solution of the forward kinematics is given by the following set of equations:

$$\tan q_3 = -\tan(q_2)/cos(q_1) \qquad (5)$$
$$sin(q_4) = sin(q_1)sin(q_3). \qquad (6)$$

As for the inverse kinematics, given a desired end-effector orientation ϕ_1 and ϕ_2, it is possible to formulate the solutions
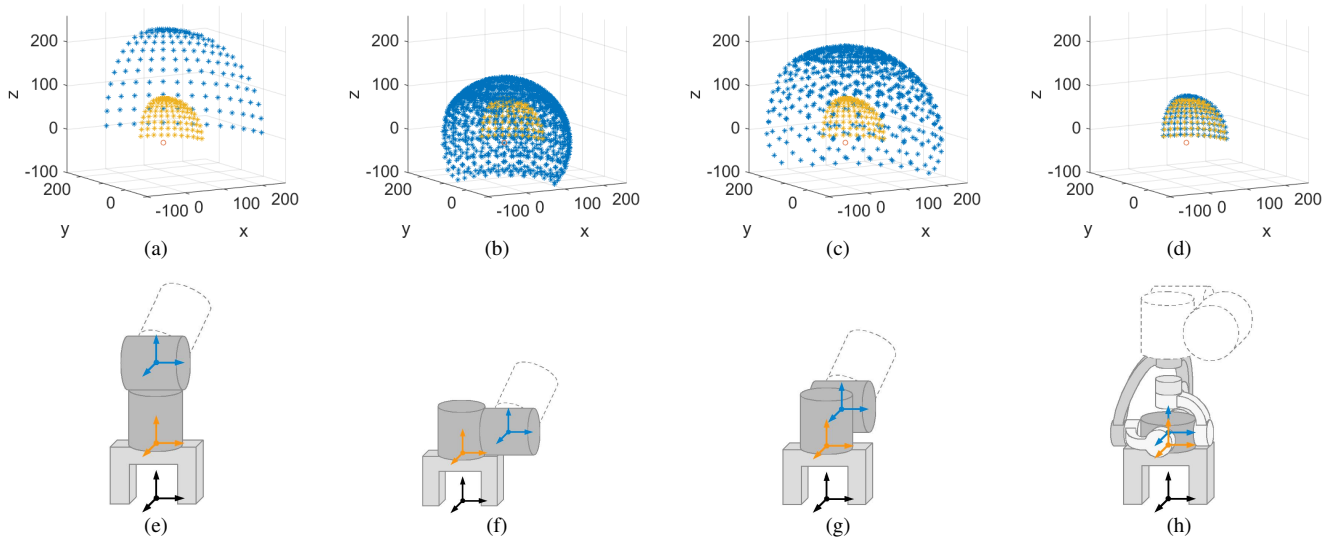
Fig. 4: Reversed workspace of different wrists layout. A spherical roll-pitch-roll wrist (4(a) and 4(e)), non-spherical roll-pitch-roll wrists (4(b)-4(c) and 4(f)-4(g)), and a parallel spherical wrist (4(d) and 4(h)). In orange is colored the end-effector flange reference frame, while in blue is represented the last reference frame of the wrist. The reference frame colors correspond to the hand and wrist reversed workspace respectively. Note that the hand envelope is the same in all the considered cases and is reported as reference to compare the different reversed workspace with respect to the human wrist. All dimensions are in mm.
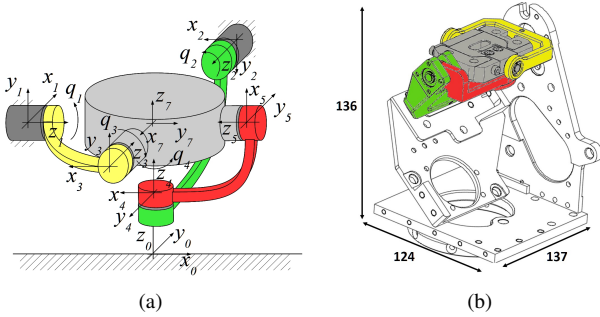

Fig. 5: Kinematic scheme and CAD drawing of the parallel 2DoFs mechanism. All dimensions are in mm.

for the active joints as,

$$q_1 = \phi_1 \quad or \quad q_1 = \phi_1 - \pi. \tag{7}$$

$$\tan(q_2) = -\tan(q_3)\cos(q_1). \tag{8}$$

where $q_3 \in \{\phi_2, \pi - \phi_2\}$. All possible solutions for equations (5), (6), (7) and (8) are deeply discussed in [13]. Fig. 5(b) shows the actual implementation of the mechanism kinematics. The yellow fork is the link of chain 1 (i.e. $\{Z_0, Z_1, Z_3, Z_7\}$) while green and red links form chain 2 (i.e. $\{Z_0, Z_2, Z_4, Z_5\}$). The gray part is the mobile platform where the end-effector is connected. The ranges of motion of q_1 and q_2 were iteratively defined. Firstly, the singularity free workspace was determined. Then, the mechanism was designed in order to find the best trade off among wrist size and range of motion. As matter of fact, the end effector shape/size determines a sub-set of the workspace, free from interferences with the mechanism structure. According to [20] wrist extension has a dominant role over flexion in

daily living manipulation activities. Therefore, a reference frame rotation of $40°$ was defined to maximize the wrist extension, which is particularly relevant for top grasp in box settings (Fig. 11). Concerning the yaw motion, the same study highlights a use of the ulnar/radial deviation of about $15°$. Therefore, the first prototype of the compact wrist implements q_1= [-80°,+30°] (flexion/extension), q_2=[-20°,+20°] (ulnar/radial deviation).

C. Jacobian Operator

According to [13], the Jacobian operator J is formulated, for the 2DOFs wrist, as

$$J = D^{-1} B. \tag{9}$$

where J maps the joint velocities to the platform Euler velocities. D is set to be equal $D_0 S$, where D_0 is the type II Jacobian matrix of the parallel structure, given by

$$D_0 = \begin{bmatrix} C_{\phi_1}C_{q_1}C_{\phi_2} + C_{\phi_2}S_{\phi_1}S_{q_1} & C_{q_2}S_{q_1}S_{q_3} \\ S_{\phi_2}S_{q_1} & C_{q_1}S_{q_3}S_{q_2} - C_{q_3}C_{q_2} \\ -C_{q_1}S_{\phi_2} & S_{q_1}S_{q_3}S_{q_2} \end{bmatrix}^T, \tag{10}$$

S is a 3×2 matrix given by,

$$S = \begin{bmatrix} 1 & 0 \\ 0 & C_{\phi_1} \\ 0 & S_{\phi_1} \end{bmatrix}. \tag{11}$$

and B is the type I Jacobian matrix, given by

$$B = \begin{bmatrix} C_{\phi_1}C_{\phi_2}C_{q_1} + C_{\phi_2}S_{\phi_1}S_{q_1} & 0 \\ 0 & C_{q_3}C_{q_2} - C_{q_1}S_{q_3}S_{q_2} \end{bmatrix}. \tag{12}$$

D. Series Elastic Actuation Module

The two DOFs of the parallel wrist are actuated by a SEA module, which consists of a brushed DC motor (Maxon DCX-22S), (1) in Fig. 6, equipped with an integrated planetary gearbox GPX22A (2) with reduction ratio (i) $35:1$, efficiency (η) 81% and a worm gearbox system A17U10 (3-4) with $i = 10:1, \eta = 59\%$, for a global ratio of $350:1$. At this stage, the maximum continuous output torque of the system is $2.36Nm$, the total efficiency of the system is 47.8%. Concerning backdrivability, note that a mechanism self-locks when its retrograde efficiency $\eta' = 2 - (1/\eta)$ is negative [21]. When there is a series of mechanism, η'_{tot} is evaluated as $\eta'_{tot} = \eta'_1 \eta'_2 ... \eta'_n$, thus, the SWR is backdrivable. Angular contact bearings (5) were selected for supporting the shaft of the worm. They serve a dual function: increase output shaft position accuracy and relieve the Maxon motor internal bearing from axial and radial loads of the transmission. The actuator has a 12 bit encoder as position sensor, located in (6) while its output is the pulley (7). Fig. 7 shows the belt transmission system used to connect the output pulley (7) and the mechanism rotation axis (11). A
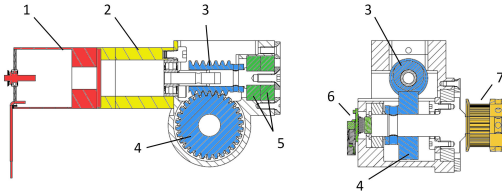

Fig. 6: Actuation module cross sections.

non-linear elastic transmission system is realized by coupling the belt tensioner with a linear spring on each side of the belt (8-9-10 Fig. 7-a). This design choice, among others, allowed to use off-the shelf components rather than custom designed springs [22]. The non-linear spring mechanism and parameters are shown in Fig. 7(b-c), while its model is defined by

$$\tau = (T_2 - T_1)r_p = K(\delta)\delta, \qquad (13)$$

where

$$
\begin{aligned}
&\delta = \theta_i - q_i, \\
&T_i = \frac{K_{lin}\ a\ x_i\ cos(\alpha_i)}{2\ b\ sin(\psi_i)}, \\
&x_i \simeq a\ \alpha_i, \\
&\alpha_i \simeq \frac{h_0 - I_p\ tan(\psi_i)/2}{b}, \\
&\psi_i \simeq atan(\frac{2\sqrt{(L_0 \pm \delta\ r_p/2)^2 - (I_p/2)^2}}{I_p}).
\end{aligned}
\qquad (14)
$$

The pulleys inter-axis (I_p) and the belt length (L) set the maximum deflection, while the spring stiffness (K_{lin}) is selected to compensate the end-effector weight $(0.5kg)$ at initial configuration $(q_1, q_2 = 0)$. Provided that the two motors
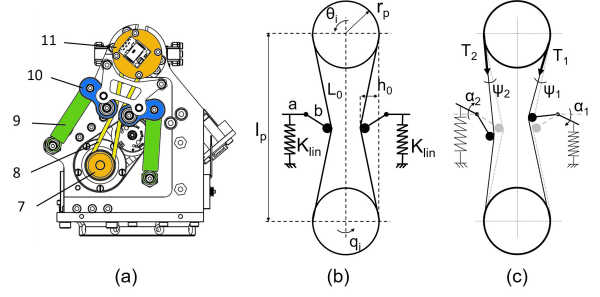

Fig. 7: Non-linear elastic transmission implementation (a) and model shown in the undeformed (b) and deformed condition (c).

have a different range of motion, the spring maximum deflection has been tuned accordingly. Belt length and pulley inter-axis are 201mm-75.5mm and 168mm-59.5mm, respectively for the two joints. Therefore, the maximum deflection δ_1 is $\pm 10°$ and δ_2 is $\pm 1°$. The distributed actuation architecture, let us locate the motors close to the wrist base, improving the compactness of the system. Finally, the Compact Soft Articulated Parallel Wrist sizes are $137mm \times 124mm \times 136mm$, as reported in Fig. 5(b). The overall wrist weight is 1.4kg and consists of 2 SEA actuators (0.35kg each), a 2DOFs joint (0.3kg) and wrist structure including connecting flanges, covers and electronics (0.4kg). The actuator module weight and size ($W \times H \times D$ $96mm \times 37mm \times 44mm$), although in a prototypical implementation, is not far from commercial actuators designs with similar specifications, e.g the Dynamixel Pro Plus[4] $M24P$-010-$S260$-R with weight $0.27kg$, size $42mm \times 72mm \times 42mm$, continuous torque of $1.7Nm$ and gear ratio $257:1$. As for the 2DOFs joint, its volume fits within a prism of dimensions $100mm \times 80mm \times 30mm$ which is compact compared with other multi-DOF parallel kinematic schemes, like the High Angle Active Link [23] whose volume fits in a cylinder of dimensions $49mm \times 48mm(D \times L)$ or the quaternion joint [24] with a volume of $60mm \times 90mm(D \times L)$ and weight $0.45kg$ (actuators excluded). The electronic board, softwares and libraries used are part of the Natural Machine Motion Initiative (NMMI) platform[5] [11]. Electronic board is used to control both actuation units. MATLAB/Simulink libraries and a ROS node can be used to control the motors. The different gains of the PI controllers for each motor are tuned based on the Ziegler-Nichols method.

E. Cartesian Stiffness Analysis

Our approach is based on the virtual joint modeling method (VJM) [25], where link compliance is modeled introducing virtual joints with 3D stiffness properties, and joint compliance is modeled by virtual springs. Under the assumption of negligible elastic deformations in the structural links (Aluminum alloy 7075-T651-Ergal) and perfect passive joints, (i.e, they have no influence on the end-effector

---

[4]http://www.robotis.us

[5]https://www.naturalmachinemotioninitiative.com/

motions [25], [26]), the Cartesian stiffness of a (not over-constrained) parallel manipulator with elasticity lumped in the active joints is mapped to the joint-space stiffness (K_θ).

According to [27] the complementary stiffness matrix is negligible with respect to K_θ, therefore

$$K_c = J^{-T} K_\theta J^{-1} = \begin{bmatrix} K_{\phi_1\phi_1} & K_{\phi_1\phi_2} \\ K_{\phi_1\phi_2}^T & K_{\phi_2\phi_2} \end{bmatrix}, \qquad (15)$$

where K_θ is given by,

$$K_\theta = \begin{bmatrix} K_1 & 0 \\ 0 & K_2 \end{bmatrix}. \qquad (16)$$

IV. EXPERIMENTAL CHARACTERIZATION

A. Experimental Setup

For joint stiffness characterization, we refer to the method proposed in [28], where the actuator link is forced to span an angle symmetrically around a vertical axis, in quasi-static conditions, inducing a spring deflection as a function of the gravitational load. We applied a sinusoidal input with frequency $0.1 rad/s$ and amplitude $[-30°, 30°]$ and $[-20°, 20°]$ to q_1 and q_2 respectively. A load of $4kg$ was connected at the end-effector flange, at a distance l of $100mm$ from the center of the platform. We measured both the link θ_i and motor position q_i. The torque on the output link is calculated as $\tau_i = m_i g l \sin(\theta_i)$.

B. Torque-deflection and stiffness characteristics

Fig. 8, shows the torque-deflection characteristics of each joint. Blue dots represent the raw deflection measurements, the red curve is the 4th order polynomial fitting of the raw data, while yellow dots represent the average among the loading and unloading curve. Hysteresis is related to the internal static friction and differs between the up and down swing, being larger in the upward motion. Hysteresis max loop amplitude is about $0.1 rad$ for the pitch motor (q_1) and $3.5e^{-03} rad$ for the yaw motor (q_2), due to the different design requirements. Fig. 9 shows the stiffness-torque characteristic of each motor. The stiffness curves are computed on the base of experimental data. First we computed a polynomial fitting of torque (τ) as function of deflection (δ), see Fig. 8, then to obtain the stiffness, we evaluated the derivative of τ w.r.t. δ (Fig. 9). The stiffness of the pitch motor varies almost linearly as a function of the external torque, while the yaw stiffness exhibits a strong non-linear behavior and tends to infinity. For an external wrench ω expressed in the reference frame as

$$\omega = \begin{bmatrix} \tau_x \\ \tau_y \\ \tau_z \end{bmatrix} = \begin{bmatrix} m g l \sin(\phi_1) \cos(\phi_2) \\ m g l \sin(\phi_2) \cos(\phi_1) \\ 0 \end{bmatrix}, \qquad (17)$$

we evaluated the cartesian stiffness at each orientation of the task space on the base of (16), built with stiffness-deflection experimental data for each DOF. In (17) m is set to $1kg$. The torque applied at the decoupled links is expressed as $\tau = J^T \omega$. To evaluate the space cartesian stiffness, we used the two indices reported in Fig. 10. Fig. 10(a) shows the ratio between the smallest eigenvalue (λ_{min}) of K_c and the largest
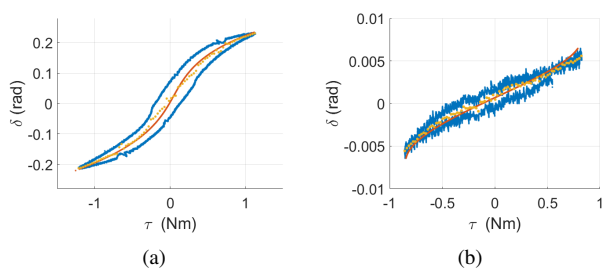

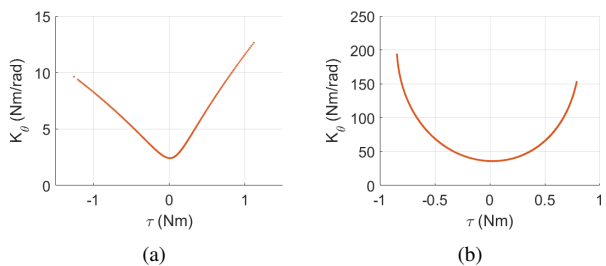Fig. 8: Hysteresis loop of pitch motor (left) and yaw motor (right).

Fig. 9: Joint stiffness of pitch motor (left) and yaw motor (right).

one (λ_{max}) over the task space orientations. Mechanism dexterity is equal to the square root of that ratio. A higher dexterity is concentrated in the mid span of the ϕ_2 axis and it decreases as we approach the boundary limits at $\phi_2 = \pm 20°$. Along ϕ_1 axis, the asymmetrical span leads to a higher dexterity around the $-40°$ orientation, dexterity decreases irregularly as we approach the boundary limits. Fig. 10(b) shows the maximum eigenvalue of the stiffness matrix over the workspace. It represents the maximum possible displacement from the equilibrium position that can occur in the task space in the direction of the corresponding eigenvector. The system loses stiffness at $[\phi_1 = -80°, \phi_2 = 0°]$ where the structure approaches singular configuration (J as well as K_c are singular around $\pm 90°$). The stiffness model in Eq. (10) serves to study the precision of a mechanism to find the most suitable design [29].

V. GRASP-IN-A-BOX EXPERIMENTS

To preliminarily evaluate the performance of the SWR, we use a physical set-up which consists of a 7DOFs Franka Emika manipulator, a Pisa/IIT SoftHand as end-effector [11],
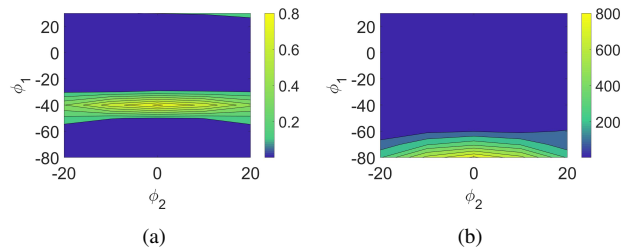

Fig. 10: Cartesian stiffness (K_c) evaluation over the wrist task space. Contour plots of (a) the ratio of K_c minimum to maximum eigenvalues ($\lambda_{min}/\lambda_{max}$), (b) K_c maximum eigenvalues (λ_{max}).

	box			shelf		
	can	box	ball	can	bottle	box
human	✓	✓	✓	✓	✓	✓
robot straight E-E	fail	fail	✓	✓	✓	fail
robot angled E-E	fail	fail	✓	✓	✓	✓
SWR	✓	✓	✓	✓	✓	✓

TABLE I: Grasp success rate.

		pitch joint	pitch defl.	yaw joint	yaw defl.
box	can	-80	8.1	3	0.97
	box	-70	3.4	6	0.34
	ball	-59	2.8	0	0.21
shelf	can	0	5.7	0	0.15
	bottle	30	6.4	-20	0.25
	box	-28	6.9	-20	0.45

TABLE II: Joint position and deflection grasping different objects in box and shelf settings. All values are in deg.

a set of objects (sphere, cylinder and box) and a shelf with cubic cells, which can be oriented both horizontally (box-like) and vertically (shelf-like). The shelves have cells dimensions $33cm \times 33cm \times 39cm (w \times h \times d)$, which are comparable with those used in the Amazon picking challenge [8]. We compared the grasp success rate of the robot in three different configurations: straight end-effector (Fig. 11(d)), end-effector connected at $90°$ (Fig. 11(g)) and end-effector equipped with the SWR (Fig. 11(j)). Human grasp is reported as a reference for each grasped object. Figs. 11-12 report the pictures of the test set and Table I summarizes the experimental results for the box and for the shelf, respectively. Table II reports the SWR actuators positions and their corresponding deflections for each grasped object and environment setting. **Experiments in the box setting:** we considered three different grasp types, a top grasp for the low cylinder with a roughly square side section (can), an angled grasp for a large box and sliding grasp for a ball (using the box side as an environmental constraint). Table I shows that the robot with both the straight and angled end-effector (E-E), fails to reach a centered object due to wrist collision against the box walls which caused E-E wrong positioning, while the robot with the SWR succeeds (Fig. 11(j)). In Figs. 11(f-i-l) all the robot configurations succeeded in grasping laterally and robustly a ball positioned next the box wall by taking advantage of the wall constraint forces. **Experiments in the shelf setting:** in this case we considered a top grasp for a low cylinder, a lateral grasp for a high cylinder (bottle), and an angled grasp for a large box. Table I shows the three robot configurations succeeding in grasping a small cylinder from a shelf with a top grasp. In figures12(e), 12(h) and 12(k), the robot succeeds in grasping laterally a longer cylindrical object (bottle). The straight E-E robot fails to grasp a box (Fig. 12(f)) due to E-E wrong positioning with respect to the object COG, caused by shelf physical constraints. The robot both in angled E-E and in SWR configurations, succeeds in grasping the box (Figs. 12(i) and 12(l)). It is worth noticing that despite a similar successful rate among the configurations, the SWR provides, in average, the largest clearance from the shelf walls. Concluding, the
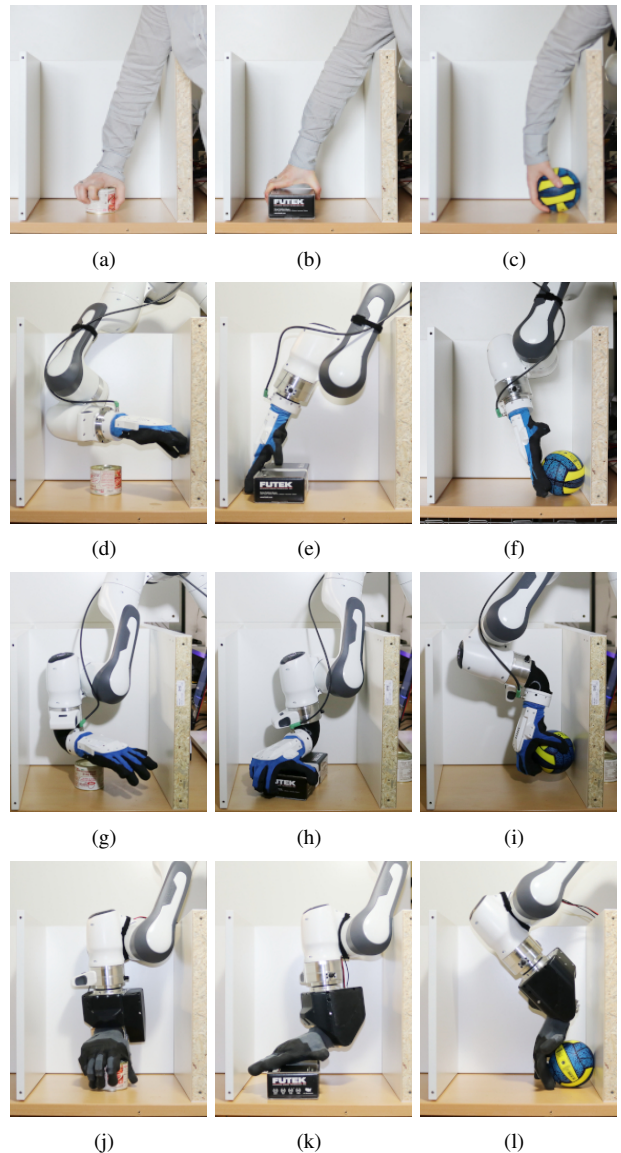

Fig. 11: Grasp experiment in box setting for different objects and manipulator configurations.

robot with SWR configuration has the highest success rate for the box setting, while has the same success rate as the angled E-E in the shelf setting. However, for this end-effector morphology, grasping from a box is much more challenging than the shelf setting, which makes the overall success rate higher for the robot with SWR configuration.

VI. CONCLUSIONS

This paper deals with the problem of increasing the dexterity of a robot arm when grasping in a box. Observation on human arm dexterity and grasp strategies, identified compactness, kinematic structure and compliance as the main characteristics which most determine the performance of human wrist. We proposed the *reversed workspace* method to study and compare robotic manipulators and consequently identify the mechanism that comes closer to the human reference. Results suggested to combine the properties of
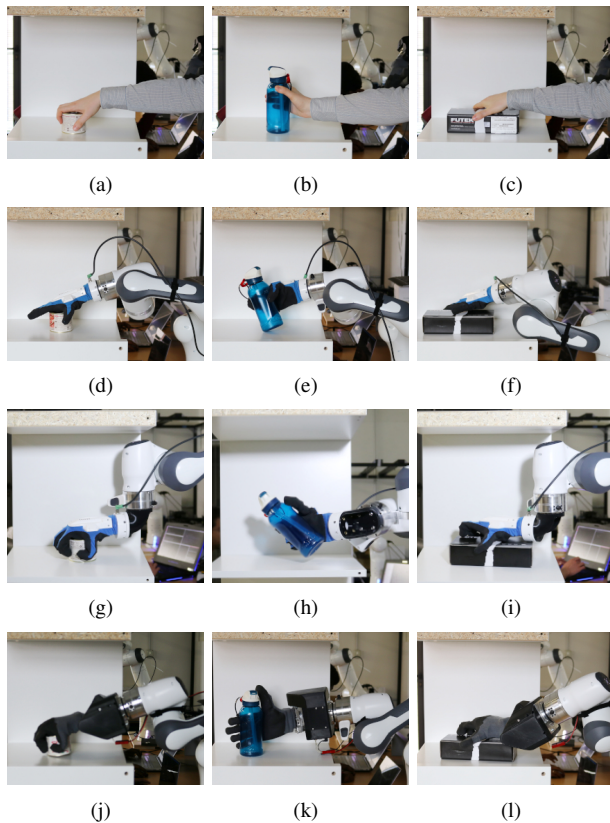
Fig. 12: Grasp experiment in shelf setting for different objects and manipulator configurations.

serial and parallel architectures, to obtain a suitable trade-off between compactness and workspace. On this base, we developed the SWR that can be easily interfaced with industrial off-the-shelf manipulators to enhance their manipulation capabilities in constrained environment. The proposed design includes a 2DOFs parallel architecture with non-linear SEA actuators. The paper reported both the model of the elastic transmission and its experimental characterization, included a model of the cartesian stiffness. Preliminary experimental validation was done comparing the grasp successful rate of a robotic manipulator with and without the SWR, in a variety of grasp scenarios, objects, shelf/box environment and end-effector orientation. The SWR showed the highest grasp success rate over the whole set of tests and often demonstrated human-like grasp strategies. These results, although at a preliminary stage, confirm the potential of this approach for addressing the grasp in a box problem. Future work will consider mechanical optimization of the SWR overall design towards its testing in real industrial use-cases. Besides this introductory work, we will focus on control and planning aspects (e.g. managing arm redundancy) in highly constrained environments.

REFERENCES

[1] R. R. Ma and A. M. Dollar. On dexterity and dexterous manipulation. In *International Conference on Advanced Robotics*, pages 1–7, 2011.

[2] Y. C. Nakamura and al. The complexities of grasping in the wild. In *2017 IEEE-RAS 17th International Conference on Humanoid Robotics (Humanoids)*, pages 233–240, Nov 2017.

[3] M. Bonilla, E. Farnioli, C. Piazza, M. Catalano, G. Grioli, M. Garabini, M. Gabiccini, and A. Bicchi. Grasping with soft hands. In *2014 IEEE-RAS Humanoids Conference*, pages 581–587, Nov 2014.

[4] Clemens Eppner, Raphael Deimel, José Álvarez Ruiz, Marianne Maertens, and Oliver Brock. Exploitation of environmental constraints in human and robotic grasping. *IJRR*, 34(7):1021–1038, 2015.

[5] C. Piazza, G. Grioli, M. Catalano, and A. Bicchi. A century of robotic hands. In *Ann. Rev. Control, Robot Autonomous System, vol. 2*, 2019.

[6] F. Montagnani, M. Controzzi, and al. Is it finger or wrist dexterity that is missing in current hand prostheses? *IEEE Transactions on Neural Systems and Rehabilitation Engineering*, 23(4):600–609, 2015.

[7] N. M. Bajaj, A. J. Spiers, and A. M. Dollar. State of the art in artificial wrists: A review of prosthetic and robotic wrist design. *IEEE Transactions on Robotics*, 35(1):261–277, Feb 2019.

[8] Nikolaus Correll, Kostas Bekris, et al. Analysis and observations from the first amazon picking challenge. *IEEE Transactions on Automation Science and Engineering*, 15(1):172–188, 2018.

[9] Nikolaus Vahrenkamp and Tamim Asfour. Representing the robot's workspace through constrained manipulability analysis. *Autonomous Robots*, 38(1):17–30, Jan 2015.

[10] Philip Long and Taskin Padir. Evaluating robot manipulability in constrained environments by velocity polytope reduction. In *2018 IEEE-RAS 18th International Conference on Humanoid Robots (Humanoids)*, pages 1–9. IEEE, 2018.

[11] Cosimo Della Santina, Cristina Piazza, and al. The quest for natural machine motion: An open platform to fast-prototyping articulated soft robots. *IEEE Robotics & Automation Magazine*, 24(1):48–56, 2017.

[12] Clement M Gosselin and François Caron. Two degree-of-freedom spherical orienting device, October 19 1999. US Patent 5,966,991.

[13] S. Mghames, M. G. Catalano, A. Bicchi, and G. Grioli. A spherical active joint for humanoids and humans. *IEEE RAL*, pages 1–1, 2019.

[14] Koichi Koganezawa, Hiroshi Inomata, and Toshiki Nakazawa. Actuator with non-linear elastic system and its application to 3 dof wrist joint. In *Mechatronics and Automation, 2005 IEEE International Conference*, volume 3, pages 1253–1260. IEEE, 2005.

[15] Fabrizio Sergi, Melissa M Lee, and Marcia K O'Malley. Design of a series elastic actuator for a compliant parallel wrist rehabilitation robot. In *2013 IEEE 13th International Conference on Rehabilitation Robotics (ICORR)*, pages 1–6. IEEE, 2013.

[16] R. Drillis, R. Contini, and M. Bluestein. Body segment parameters: A survey of measurement techniques. *Artificial Limbs*, 8:44–66, 1964.

[17] Divya Shah and al. A comparison of robot wrist implementations for the icub humanoid. *Robotics*, 8(1):11, 2019.

[18] Yuefa Fang and Lung-Wen Tsai. Structure synthesis of a class of 3-dof rotational parallel manipulators. *IEEE transactions on robotics and automation*, 20(1):117–121, 2004.

[19] YD Patel and PM George. Parallel manipulators applications—a survey. *Modern Mechanical Engineering*, 2(03):57, 2012.

[20] Andrew K Palmer and et al. Werner. Functional wrist motion: a biomechanical study. *Journal of Hand Surgery*, 10(1):39–46, 1985.

[21] U. Meneghetti E. Funaioli, A. Maggiore. Lezioni di meccanica applicata alle macchine, vol. i. *Patron Editore, Bologna*, 1987.

[22] Bram Vanderborght and al. Variable impedance actuators: A review. *Robotics and autonomous systems*, 61(12):1601–1614, 2013.

[23] Keisuke Sone, Hiroshi Isobe, and Koji Yamada. High angle active link. *Special Issue Special Supplement to Industrial Machines*, 2004.

[24] Y. Kim, J. Kim, and W. Jang. Quaternion joint: Dexterous 3-dof joint representing quaternion motion for high-speed safe interaction. In *2018 IEEE/RSJ International Conference on Intelligent Robots and Systems (IROS)*, pages 935–942, Oct 2018.

[25] Alexandr Klimchik. *Enhanced stiffness modeling of serial and parallel manipulators for robotic-based processing of high performance materials*. PhD thesis, Ecole Centrale de Nantes (ECN); Ecole des Mines de Nantes, 2011.

[26] Clement Gosselin. Stiffness mapping for parallel manipulators. *IEEE Transactions on Robotics and Automation*, 6(3):377–382, 1990.

[27] J Kenneth Salisbury. Active stiffness control of a manipulator in cartesian coordinates. In *IEEE conference on decision and control including the symposium on adaptive processes*, pages 95–100, 1980.

[28] G Grioli, S Wolf, M Garabini, M Catalano, et al. Variable stiffness actuators: The user's point of view. *IJRR*, 34(6):727–743, 2015.

[29] Dan Zhang. *Parallel robotic machine tools*. Springer Science &
Business Media, 2009.